Chemical composition and mass emission factors of candle smoke particles

Pagels, Joakim; Wierzbicka, Aneta; Fors, Erik; Isaxon, Christina; Dahl, Andreas; Gudmundsson, Anders; Swietlicki, Erik; Bohgard, Mats

Published in:
Journal of Aerosol Science

DOI:
10.1016/j.jaerosci.2008.10.005

2009

Document Version:
Peer reviewed version (aka post-print)

CHEMICAL COMPOSITION AND MASS EMISSION FACTORS OF CANDLE SMOKE PARTICLES

JOAKIM PAGELS[1,*], ANETA WIERZBICKA[1], ERIK NILSSON[1,2], CHRISTINA ISAXON[1], ANDREAS DAHL[1], ANDERS GUDMUNDSSON[1], ERIK SWIETLICKI[2] AND MATS BOHGARD[1]

1. Ergonomics and Aerosol Technology (EAT), Lund University, P.O. BOX 118, SE-221 00 Lund, Sweden.

2. Nuclear Physics, Lund University, P.O. BOX 118, SE-221 00 Lund, Sweden.

*Corresponding author. Tel.: +46-46-222-16-88; fax: +46-46-222-44-31

E-mail address: joakim.pagels@design.lth.se (J. Pagels)

KEYWORDS: AEROSOL, CANDLES, INDOOR AIR, SOOT, MASS CLOSURE, ULTRAFINE PARTICLES

Abstract

The aim of this study is to investigate the physical and chemical properties of particle emissions from candle burning in indoor air. Two representative types of tapered candles were studied during steady burn, sooting burn and smouldering (upon extinction) under controlled conditions in a walk-in chamber. Steady burn emits relatively high number emissions of ultrafine particles dominated by either phosphates or alkali nitrates. The likely source of these particles is flame retardant additives to the wick. Sooting burn in addition emits larger particles mainly consisting of agglomerated elemental carbon. This burning mode is associated with the highest mass emission factors. Particles emitted during smouldering upon extinction are dominated by organic matter. A mass closure was illustrated for the total mass concentration, the summed mass concentration from chemical analysis and the size-integrated mass concentration assessed

from number distribution measurements using empirically determined effective densities for the three particle types.

1. Introduction

A significant fraction of the exposure to fine and ultrafine particles occurs indoors in the home and other indoor environments, as people spend more than 85% of the time in indoor environments (Klepeis et al. 2001). The indoor exposure includes particles infiltrating from outdoor air and indoor particle sources. Many epidemiological studies linking particle exposure to adverse health effects have been made in outdoor air, partly due to the relative ease of using data from central monitoring stations outdoors in large populations within a city. While the characteristics of ambient particles have been studied extensively, the contributions to the exposure from individual indoor particle sources are poorly known. There may also be significant differences between particles of indoor and outdoor origin in terms of particle chemical composition, size distribution and morphology, properties likely to be important in controlling adverse health effects.

In several field studies in homes, candles have been identified as sources of ultrafine particles (Matson 2005, Hussein et al. 2006, Wierzbicka et al. 2008), larger accumulation mode particles (Ogulei et al. 2006, Long et al. 2000) and a major contributor to indoor Elemental Carbon (EC) and $PM_{2.5}$ concentrations (Sörensen et al. 2005, Larosa et al. 2002). Candle burning has also been associated with black spot formation on walls and staining of ancient paintings, sculptures and tapestries in churches (Hyunh et al. 1991; Edwards et al. 2005; Perez et al. 1999).

Candles have been used since ancient times as a source of light and are today commonly used for aesthetic and religious purposes in various indoor environments. Already in 1860 Michel Faraday described mechanisms of the combustion taking place in a candle flame in his lecture notes on “the chemistry of candles”. The candle flame can be approximated as a diffusion flame, with the wax serving as fuel and the wick serving as transport mode of the fuel by capillary forces. Air is the oxidant, transported by

convection vertically along the flame. In fuel rich regions of the flame, large quantities of soot particles form. The yellow incandescent light making up the majority of the flame is the result of soot oxidation in the flame. During normal steady burn, in principle all soot formed in the flame can be oxidised, resulting in very low EC emissions. However, horizontal air movements in the vicinity of the flame, for example due to an open window, may result in a flickering flame and some soot being able to escape without being oxidised. This we refer to as sooting burn mode. Another mode of burning is smouldering upon extinction of the candle producing visible white smoke.

There are several different types of additives used in candles to improve the burning performance and aesthetic appearance (Knight et al. 2001). For example alkanoic acids such as stearic acid are used to improve hardening characteristics of the wax and increase the melting point. Added colouring pigments may contain heavy metals. Inorganics such as ammonium phosphates and borax (a salt mixture containing borates) are added to the wick to act as a flame retardants to ensure that the wick is consumed at a sufficient rate and to prevent glowing of the wick upon extinction. In certain types of candles, metals such as zinc, tin and lead are added to the wick to improve mechanical stability. More recently fragrance oils have been added to certain types of candles.

A potential health problem related to candle burning is the occurrence and release of metal additives from the wick and colour pigments. Several studies have focused on lead and other heavy metal emissions from metal-cored candles (Van Alphen 1999, Nriagu and Kim 2000, Wasson et al. 2002, Lin et al. 2003). Wasson et al. (2002) found relatively high lead emission rates of 0.1-1.7 mg h^{-1} in 8 out of 100 purchased candles. Burning of such high emitting candles can easily lead to exceedance of ambient air lead concentration limits, for example 1.5 µg m^{-3} set by the US EPA. They also showed that 8-23% of the lead in the wick was released as fine particles, while the rest was retained in the ash in the wax pool. For example in the USA, candle wicks containing lead are uncommon after agreements between national manufacturers to discontinue the use of lead as a core material (Knight et al. 2001). Replacements for lead

in metal-cored candle wicks include zinc and tin. Zinc emission factors up to 0.12 mg h^{-1} were identified by Nriagu and Kim (2000).

Lau et al. (1997) investigated emissions of Polycyclic Aromatic Hydrocarbon (PAH) emissions and gas-phase Volatile Organic Carbon (VOC). They found that candles have low PAH and VOC emission levels compared to other indoor combustion sources. This is likely caused by the high combustion temperature and relatively complete combustion occurring in a steady burning candle.

Li and Hopke (1993) studied particle emissions from a steady burning single paraffin wax candle and found that the initial size distribution was dominated by ultrafine particles of around 30 nm in diameter. Their study focused on the hygroscopic growth of particles measured at a relative humidity similar to that occurring in the human respiratory tract. They found diametric hygroscopic growth factors of around 2.2 at RH=99.0-99.5%, which is significantly higher than for most known organic compounds and elemental carbon. They speculated that the presence of organic acids were responsible for the high particle growth.

Afshari et al. (2005) studied number concentrations emitted from two “pure wax” candles and two scented candles separately in a 32 m^3 chamber (air exchange rate 1.7 h^{-1}) and found maximum number concentrations of 240000 particles cm^{-3} and 69000 particles cm^{-3} respectively, for the two candle types measured with a condensation particle counter (particles > 20 nm).

Fine, Cass and Simoneit (1999) focused on detailed analysis of organic compounds present in the particle phase of emissions from a paraffin and a beewax candle. They found that sooting burn conditions are associated with relatively high elemental carbon emissions. During sooting burn an additional larger sized particle mode above 100 nm appears in mobility size distribution measurements in addition to the ultrafine mode. Organic carbon emissions were mainly associated with smouldering burning upon candle extinction; similarly a larger mode above 100 nm occurred during smouldering. Gravimetrically

determined emission factors associated with extinguishing one candle were 0.6-1.8 mg, while sooting burn led to an emission factor as high as 26 mg h^{-1}. Through detailed GC/MS analysis they showed that the particle phase organics in the candle smoke consist of a combination of unaltered fuel which has undergone evaporation and condensation and partly oxidized fuel. There were relatively large differences in organic composition between the paraffin and the beewax candle smoke, due to differences in the fuel composition. Based on their data the chemical composition of the small ultrafine particles dominating the "efficient burning" mode could not be determined.

Fan and Zhang (2001) used a nephelometer to assess mass emission factors of 3.4 mg h^{-1} for unscented 7.6 cm diameter paraffin candles. Zai et al. (2006) used another nephelometric device to determine emission factors of a single tapered candle made of paraffin wax during three different burn conditions. During steady burn, emission factors were low (0.33 mg h^{-1}), while higher emissions of 7.6 mg h^{-1} were found during sooting burn. However, the response of nephelometers depends strongly on the optical particle properties which in turn are a strong function of particle size, morphology and chemical composition. Particularly the response to ultrafine particles (d_p<100 nm) is very low compared to larger sizes.

Although efforts have been made to characterize particle emissions from candles in several studies, there are still significant knowledge gaps, especially regarding the composition and concentration of particles emitted during the different modes of burning. For example, the composition of the ultrafine particles which appear in very high number concentrations during steady burning is not known. To our knowledge no study has performed measurements of inorganics (except for heavy metals such as lead and zinc) which are present in the candle as additives and may become airborne through volatilization and condensation or through heterogeneous reactions in the gas-phase. Furthermore, there are no reported studies of the morphology of particles from different burning conditions.

The aim of this paper is to investigate the chemical composition, morphology and mass emission factors during three different modes of burning. Another aim is to establish effective density factors to allow assessments of the particle mass size distribution using a Scanning Mobility Particle Sizer and to compare mass concentrations using different instrumental approaches.

2. Materials and Methods

2.1. Experiment chamber

Candle smoke was generated in a 21.6 m^3 stainless steel chamber (Figure 1). The RH in the chamber was controlled to 30 ± 5% and the temperature was 23-28 °C. The temperature typically increased during an experiment due to the energy released as heat from the candles. The supply air flow rate was determined from pressure drop measurements at the entrance to the chamber. The flow rate was 10.8 m^3 h^{-1}, which corresponds to an air exchange rate of 0.5 h^{-1}. The supply air passed an activated carbon filter to remove VOCs and oxidants and an ULPA (Ultra Low Penetration Air filter) particle filter. Air to the chamber was supplied from the roof while the exhaust was positioned in the opposite corner from the supply at a height of 0.5 m from the floor. The exhaust fan was adjusted until a positive pressure difference between the chamber and the surrounding air of 5-10 Pa was established. Inside the chamber a revolving fan (model A540, Appliance Inc.) was operated to ensure complete mixing. The fan was operated at the lowest internal setting and 110 V on an external voltage supply. The resulting air velocity in the vicinity of the candles was varying in a cyclical manner with a period of 25 seconds. The peak air velocity over the cycle measured with an air velocity meter (model 8330, TSI Inc.) was 0.4 m s^{-1}. In between these peak velocities the flow rate dropped to below 0.01 m s^{-1}. We believe these cyclic air velocities mimic typical indoor convective air motion reasonably well.

The degree of mixing in the chamber was found to be complete as verified using simultaneous trace gas (SF_6) measurements (model 1312 Photoacoustic Multi-gas Monitor and model 1303 Multipoint Sampler and Doser, Innova AirTech Instruments) in three positions of the chamber. The chamber is entered

through an antechamber. The ventilation system is set up in such a way that the air leaves the main chamber through the exhaust, then enters the antechamber and finally is vented away. This ensures that the pollutant concentration is similar in the chamber and the antechamber, which in turn allows for an operator to enter the chamber with minimum disturbances of the pollutant concentration in the main chamber.

2.2. Candle emission experiments

Two different kinds of tapered candles were studied. Candles of type I were white and according to the manufacturer a wax based on pure stearin is used. Candle I is in a slightly higher price range and is marketed as a low soot emitting candle. According to the manufacturer type II candles are made up of a wax consisting of a combination of stearin and paraffin. These candles are dark blue. Candle II is a typical budget candle in a lower price range. Both candles are manufactured by market leading companies in Sweden.

In each experiment, four candles of either type I or type II were put in candle holders on a table and burned in the chamber. Three types of experiments were conducted: 1) “Steady burn” experiments, where each candle was shielded from the convective air flows from the mixing fan using 350 mm diameter, 600 mm high metallic tubes made from conventional ventilation ducts. Two candles were put inside each tube at a distance of more than 100 mm from each other. The flame was at a height of 100 mm or more, below the top of the metal tube. A 10 mm high opening was used at the bottom of each shielding tube. This reduced the degree of flickering of the flame. 2) “Sooting burn” experiments without the shielding tubes to study the influence of convective air currents on soot formation. The candle flames were flickering in these sets of experiments and 3) “Smouldering” experiments to study the white smoke emitted upon extinction of the candles. “Steady burn” and “sooting burn” experiments were performed for both types of candles, while “smouldering” experiments were only performed for candle II. All experiments were repeated two to three times.

The experimental procedure involved first ventilating the chamber to a particle concentration below 1000 particles cm^{-3} (corresponding to a mass concentration of less than 0.1 μg m^{-3}). An operator then entered the chamber after waiting 20 s in the antechamber. In the chamber, the four candles were lighted using a propane lighter (Multi-purpose lighter, BIC Inc.). Control experiments showed that this lighter does not produce any detectable amount of particles larger than 10 nm. Particle size and mass concentration measurements were started when the chamber was empty and then run continuously throughout each emission experiment. Typically, filter measurements were started 15 min after the candles were ignited, to allow build-up of particle concentrations in the chamber. Filter collection lasted 10-20 min in sooting burn experiments and 60-80 min in steady burn experiments (to compensate for the difference in emission factors). In smoulder experiments the candles were ignited and burning with shielding tubes for 10 minutes. Then the candles were extinguished using an inverted cup designed for this purpose. Each candle was covered for 3 seconds before the inverted cup was removed. Filter collection started 5 minutes after candles were extinguished and lasted for 45 minutes.

2.3. Box model for determination of emission factors

A simple box model was used to estimate mass emission factors (Koutrakis et al. 1991) from the measured particle concentrations in the chamber. In a well-mixed box the following mass conservation relationship applies:

$$\frac{dC(t)}{dt} = aC_{inc.} + \frac{E_{r,m}}{V} - (a+k)C(t) \qquad (1)$$

Where $C(t)$ is the mass concentration in the chamber, $C_{inc.}$ is the concentration in the incoming air, a is the air exchange rate (h^{-1}), k is the sum of other loss mechanisms (h^{-1}), for example wall losses, $E_{r,m}$ is the mass emission factor (mg h^{-1}) and V is the volume of the chamber. It should be noted that k typically is

particle size dependent. In our experiments the concentration in the incoming air was negligible (below 0.01 μg m^{-3}) so C_{inc} could be set to zero. Assuming that the initial concentration is zero and that $E_{r,m}$ is constant over time, Eq. 1 has the following solution:

$$C(t) = \frac{E_{r,m}}{V\,(a+k)} \cdot \left(1 - e^{-(a+k)t}\right) \qquad (2)$$

The total loss rate $(a+k)$ as a function of particle size was determined from decay experiments at low concentrations (< 5 000 particles cm^{-3}), where coagulation can be neglected (coagulation is a mass conserving loss mechanism, which should not be included in k when calculating mass emission factors). All factors on the right-hand side except the emission factor are then known. These experiments were made in connection to the real sooting burn emission tests. After filter sampling was finished, the chamber was express ventilated for about 15 min (AER 15 h^{-1}), in this time some small particles were lost through coagulation but the size distribution was still qualitatively similar to the high concentration tests.

For on-line measurements $E_{r,m}$ was fitted to experimental data using Eq. 2. For chemically resolved off-line filter experiments, first the (average) measured mass concentration over the measurement interval was calculated. The predicted average concentration over the measurement period was then calculated using the model and $E_{r,m}$ was finally varied until the measured and modelled average concentrations agreed. This approach gives the average emission factor over the measurement interval. The value of $a+k$ used in Eq. 2 was determined using the average mass geometric mean diameter determined from SMPS measurements for a given experiment. At 100 nm the value of $a+k$ was 0.65 h^{-1} indicating that the major loss rate was due to the ventilation system. At 30 nm $a+k$ increased to 1.2 h^{-1}. Emission factors were derived over the time-intervals of the filter measurements to allow comparison between the different techniques. This was typically done over the first two hours of an experiment. Note that equilibrium concentrations in the chamber are not reached at this time.

2.4. Particle characterization

The mobility particle size distribution was measured using an electrical mobility spectrometer (SMPS 3934, TSI Inc.). The instrument consisted of a bipolar charger (^{63}Ni approximate Nt-product 2 x 10^8 cm^3/s), a long column Differential Mobility Analyzer (LONG DMA, TSI Inc.) and a Condensation Particle Counter (CPC model 3010, TSI Inc.). It was used in a closed loop set-up with a sheath flow rate of 2.4 lpm and an aerosol flow rate of 0.4 lpm. These flows enabled measurements of a particle size range between 16 and 1000 nm. The size range up to 1000 nm was important in determining mass size distributions of soot and smoulder particles. The scan times were 180 s up and 30 s down. Critical orifices were used in the closed loop downstream the DMA and downstream the CPC to assure stable flows. A make-up flow of 0.6 lpm which passed a High Efficiency Particulate Air (HEPA) filter was used to add up to the nominal CPC flow rate of 1.0 lpm. The make-up flow rate, the DMA inlet flow rate and the sheath flow rates were measured using a bubble flow meter (medium cell, Gillian Inc.) before and after each experiment.

In a few experiments a Thermodesorber (TD) was added upstream the SMPS system. We refer to this combination as Volatility-SMPS. The TD enabled us to evaporate volatile particle constituents in the temperature range 30-450 °C. The TD is similar to that described by Burtscher et al. (2001). In this set-up the SMPS consisted of a long DMA and an ultrafine CPC (model 3025, TSI Inc.). The DMA was operated with a sheath flow rate of 20 lpm and an aerosol flow rate of 1.5 lpm. The measurement range of this system was 7-200 nm. A computer controlled switching valve was used to allow a measurement sequence involving one Volatility-SMPS scan passing the TD followed by two scans with the sample bypassing the TD. This sequence was repeated for six TD temperatures between 30 ºC and 425 ºC. The size-integrated particle effective volume concentration was calculated for TD and by-pass measurements, respectively. Finally the remaining non-volatile volume fraction as a function of temperature was determined from the

ratio of the calculated effective volume concentrations. In Volatility-SMPS measurements, emissions from burning of a single candle were studied; all other parameters were similar to those described above.

A correction for diffusion losses in the DMA (Martinsson et al. 2001), connectors and thermodesorber was applied to all measured data. Also an empirical size independent correction for losses due to thermophoresis at the outlet of the TD was applied (4% losses per 100 °C in temperature difference between the set temperature and the ambient temperature). These correction factors turned out to be very important, especially for particle sizes below about 20 nm during the Volatility-SMPS measurements.

A Tapered Element Oscillating Microbalance (TEOM; model 1400a, R&P Inc.) was used to determine the integrated particle mass concentration on-line. The instrument was operated at 40 °C to decrease losses of volatile organic carbon and yet be able to operate at a low relative humidity to decrease influences from water adsorption to the filter material. The instrument was equipped with a $PM_{2.5}$ inlet.

Samples for elemental and organic carbon (OC/EC) and major ions were collected using a set-up which involved first passing the sample through a PM_1 cyclone and then collection onto three different filters (Wierzbicka et al. 2005). Two parallel sampling lines were used. One line consisted of a quartz fibre filter (Tissuequartz, SKC Inc.). In the second line a Teflon filter (Zeflour, SKC Inc.) followed by a quartz backup filter (Figure 1) was used. The nominal flow rate in both lines was 5.0 lpm. These flows were controlled by needle valves operated as critical orifices and were measured before and after each experiment using the bubble flow meter.

Prior to the experiments, the quartz fibre filters were pre-heated for four hours at a temperature of 900 °C to remove organic impurities. The filters were mounted in 37 mm cassettes (3-section clear polystyrene, SKC Inc.). Stainless steel support pads were used. The filter cassettes were stored before and after the

experiments at a temperature of 5 ºC. A 0.495 cm^2 filter punch was obtained from each quartz filter and used for the OC/EC analysis. The OC concentration detected on the back-up quartz filter was subtracted from the OC concentration on the front quartz filter to correct for the positive artefact caused by adsorption of gas-phase organics onto quartz filters. A thermal-optical method, using a carbon analyzer developed by the Desert Research Institute was used for OC and EC analysis (Model 2001, DRI; Chow et al. 1993). The Teflon filters were analysed for major water-soluble ions (F^-, Cl^-, SO_4^{2-}, NO_3^-, PO_4^{3-}, Na^+, $K,^+$ NH_4^+, Ca^{2+}, Mg^{2+} and Li^+) using ion-chromatography.

A stacked filter unit sampler (Heidam et al. 1981) was used to collect particles for Particle Induced X-Ray Emission (PIXE) analysis. Polycarbonate filters (diameter 47 mm) with pore sizes of 8 μm and 0.4 μm were used in the first and second filter stages respectively. In the first stage, particles larger than about 2.5 μm are collected, while smaller particles are collected in the second stage.

A small deposit area low-pressure cascade impactor (SDI Impactor) was used to collect size-fractionated samples for PIXE analysis. The impactor divides the incoming particles into 12 stages dependent on the aerodynamic equivalent diameter and covers the particle size range 45 nm to 10 μm. The impactor flow rate is 11 lpm. Each experiment lasted 60 minutes.

Samples for Transmission Electron Microscopy (TEM) were collected onto electron microscopy-grids using an electrostatic precipitator (NAS model 3089, TSI Inc.). The sample first passed an external unipolar charger to increase the average particle charge and thereby increase the collection efficiency. The morphology of the candle particles was studied using a 300 kV transmission electron microscope (model 3000F, JEOL Inc.).

2.5. Method to determine mass size distributions using combined SMPS and TEOM data

A model was used to make a mass closure between TEOM, filter measurements and the SMPS measurements. To determine the SMPS mass size distribution, the SMPS number size distribution in each experiment was first weighted by "effective volume". The effective volume, V_{eff}, of a particle is given by

$$V_{eff}=d_p^3 \cdot \pi/6 \quad (3)$$

where d_p is the mobility diameter. The effective volume equals the true volume for spherical particles with no voids but exceeds the true volume for non-spherical particles. Three lognormal modes were fitted to the effective volume distribution. A least-squares, non-linear method was used to fit the three different parameters for each mode ($V_{eff,n}$, GMD_n, and GSD_n) to the size distribution data. To determine the mass size distribution, these lognormal modes were assigned different empirically determined effective densities, ρ_{eff}, (the particle mass, m, is given by $m=\rho_{eff} \cdot V_{eff}$). For soot particles a size dependent effective density was used (Park et al. 2003).

In calculating the particle mass from SMPS number distributions, instrumental errors both from number concentration measurements and particle sizing contributes to the overall uncertainty. Particularly, the sizing error can cause a substantial uncertainty in particle mass and effective density determinations due to the cubic dependence of particle diameter. To minimize such errors the instrument combination of SMPS and TEOM was calibrated using liquid spherical Di-ethyl-hexyl sebacate (DEHS) aerosol. Calibration aerosol was generated using an evaporation-condensation method (model SLG-270, TOPAS Gmbh) operated without seed-aerosol. An aerosol with a mass median diameter of 150 nm and a Geometrical Standard Deviation (GSD) of 1.4 was generated. The size distribution of the aerosol was completely within the measurement range of the SMPS. The experimentally found density of DEHS was calculated from the TEOM mass concentration divided by the SMPS volume. It was compared with the known density (0.91×10^3 kg m^{-3}). A correction factor was derived to correct for a slight missmatch between the

two instruments. It was typically on the order of 1.2 and was applied to all mass and effective density data involving the SMPS.

3. Results and Discussion

3.1 Particle number concentration and size distribution

Average number weighted size distributions from steady burn and sooting burn experiments are given in Figure 2. It can be seen that high number concentrations of ultrafine particles (< 100 nm) were generated. The total measured particle number concentration (16-1000 nm) was 1.14×10^6 particles cm^{-3} for candle I and 0.51×10^6 for candle II during steady burning. During sooting burn it was 0.89×10^6 and 0.27×10^6 particles cm^{-3} for candle I and II, respectively. In steady burn experiments, freshly generated ultrafine particles occurred in the peak with GMD of 20-30 nm, while the larger sizes up to about 150 nm are caused by growth, mainly from coagulation as the aerosol ages in the chamber.

In sooting burn experiments without the flow shield, the concentration in the "soot mode" with a GMD of 270 ± 30 nm (GSD 1.73 ± 0.08) increased by about two orders of magnitude in comparison to steady burn. Fine et al. (1999) and Zai et al. (2006) also found a larger sized mode during sooting burn. The number concentration in the ultrafine mode was lower in sooting burn compared to steady burn, especially for candle II. This was likely due to coagulation of formed ultrafine particles with soot mode particles.

In the smoulder experiments, the candles were burning steady for 10 minutes with flow shields. After that they were extinguished. Only candle II was studied. The influence of extinguishing the candle on the number size distribution is given in Figure 3. The particles in the ultrafine mode were mainly emitted during the period of steady burning. Upon extinction a strong increase in the concentration of particles in the larger mode with GMD 335 ± 30 nm (GSD 1.56 ± 0.04) was found.

We believe that computing number emission factors for these data would not be fully relevant. Number emission factors derived with four candles burning in these experiments would be strongly affected by coagulation. For example, the apparent number emission factor for each of the four candles would be

lower than in an experiment with a single candle. In a real setting the internal volume would be larger, decreasing the magnitude of coagulation leading to a higher apparent number emission factor. Coagulation also causes particle sizes in the chamber to increase, especially for the ultrafine mode compared to burning of a single candle. Coagulation decreases the particle concentration both in the plume just above the candle on short time-scales and upon dilution in the room air on longer time-scales.

Ultrafine particles emitted in typical indoor environments may be effectively scavenged by coagulation with larger particles in indoor air. However, the number emission factors from candles are so high that elevated concentrations of ultrafine particles will be present in most indoor environments. However, very high concentrations of accumulation mode particles from sooting burn or other strong indoor sources, may act as a very strong scavenger and then most ultrafine particles would quickly coagulate with pre-existing particles.

3.2. Particle morphology

Particles emitted during sooting burn were collected onto EM grids and the morphology was studied using TEM. In Figure 4, representative samples are shown at different degrees of magnification. The particles were highly agglomerated, with clearly discernable primary particles. Similar morphology and sizes were identified in samples from both candles I and II. The average primary particle diameter was 25-30 nm, similar to soot in diesel exhaust (Park et al. 2004). One difference compared to diesel soot is that the mobility diameter of candle soot is on the order of 270 nm while that for diesel soot is on the order of 60-80 nm (Sakurai et al. 2003). Thus, candle soot aggregates consist of a higher average number of primary particles in each aggregate compared to diesel soot. Most particles found in the TEM analysis were aggregate particles similar to those in Figure 4 with maximum lengths in the range 200-500 nm and maximum widths at 90° angle to the maximum length of around 100-350 nm. The mobility diameter is reasonably close to the average of the maximum length and the width (Park et al. 2004). Therefore the qualitative results of the TEM analysis are in reasonable agreement with the GMD of the soot mode

particles (270 nm), determined with the SMPS. Smouldering particles were, as expected, liquid and volatile and therefore difficult to analyze using TEM.

We found lower numbers of particles with sizes corresponding to the ultrafine mode in the TEM analysis than expected from the SMPS measurements. A small number of crystalline graphite particles with diameters 5-30 nm were found. We hypothesize that the majority of ultrafine particles were evaporated upon absorption of energy from the electron beam in the microscope. This would by necessity imply that the ultrafine particles have low soot content (soot is non-volatile in TEM). Another explanation could perhaps be that the collection and transport efficiency of the used sampling system is low for particles in the size range 20-30 nm. For example the 15-25 nm particles in the nucleation mode may have been lost in the unipolar charger or not efficiently collected onto the TEM-grids in the ESP. However, future studies should focus on identifying the ultrafine particles using TEM, for example using low beam intensities.

3.3. Chemical composition and mass emission factors of candle emissions

In Figure 5, mass concentrations of elemental carbon, organic matter and inorganic compounds are given for the five different cases studied. The class of inorganic compounds given in Figure 5 is the sum of all compounds detected with IC and PIXE. Inorganic matter can dominate the composition of candle smoke emissions when emissions are dominated by the ultrafine mode. This is the case for both candles during steady burning.

During sooting burn, the concentration of elemental carbon increased by more than an order of magnitude. The paraffin/stearin candle (candle II) had significantly higher EC emissions than the pure stearin candle (candle I). The experiments during sooting burn illustrate that elemental carbon concentrations emitted from candles can be very high. In these experiments simulating a small room with relative low air exchange rate, mass concentrations were up to 2000 $\mu g\ m^{-3}$ when four candles (candle II) were burned.

In smouldering experiments the particle composition was dominated by organic matter. The organic particle emissions associated with extinguishing the candles one time, resulted in average concentrations of about 100 $\mu g/m^3$ over the hour following the extinction. This is much lower compared to EC emissions during sooting burn. To obtain the organic matter concentration, the organic carbon concentration was multiplied by 1.2. Fine et al. (1999) suggested using the factor of 1.2 due to the low fraction of oxygen in wax and slightly oxidized wax molecules making up the organics released during smouldering. The concentrations reported in Figure 5 are high compared to most real indoor environments, since larger rooms are often used. Also pollutants will disperse through open doors between different rooms. Deposition onto indoor surfaces are likely larger in field experiments compared to the chamber.

Mass emission factors corresponding to the data described above were fitted using the box model. An example for TEOM data during an experiment with steady burn of candle II is illustrated in Figure 6. Two different models to correct for wall losses are compared, a model where the average GMD of the whole experiment was used to calculate the losses and a method where the evolving GMD from each SMPS scan was used. Both methods agree well with experimental data and it was concluded that the emission factors could be treated as constant over time in each experiment. The two methods agree to about 1% in fitted emission factor. As the experiment showed in Figure 6 represents the largest variation over time in GMD, it was concluded that the model with average GMD in each experiment was sufficient for the remaining data-set. Fitted mass emission factors are given in Table 1 (steady and sooting burn) and Table 2 (smouldering). Total mass concentrations were determined independently using the TEOM rather than by just summing the concentrations from the different filter analysis. The total mass emission factors determined in this study (0.9-25.3 mg h^{-1}) are significantly higher than those given by Zai et al. (2006). Particularly during steady burn we found emission factors 4-7 times higher than those reported by Zai et al.. This could be due to the use of a nephelometer by Zai et al. to assess mass concentrations. Nephelometers have a very low response to the particles smaller than about 100 nm dominating emissions during steady burn.

The mass emission factors for candle I during sooting burn in this study are similar to the results given by Zai et al., while that of candle II is three times higher. On the other hand Fine et al. reported mass emission factors close to the emission factor of candle II during sooting burn. EC is the dominant component in both the present and Fine et al.'s study. It should be noted that EC emissions are a function of the air velocity in the room and therefore very strong variations are expected under real-world conditions. In previous reports (Zai et al. 2006 and Fine et al. 1999) no measurements of air-velocities disturbing the flame during sooting burn were given, so a direct comparison is not possible to make.

Also during smouldering we found higher emission factors in this study compared to the Zai et al. study (0.72 mg compared to 0.24 mg of particles emitted each time a candle is extinguished). Fine et al. (1999) found similar emission factors to our data for a paraffin candle but more than two times higher for a beeswax candle. Perhaps additives to the wick, such as flame retardants have an influence on the smouldering time and emission levels.

3.4 Detailed inorganic composition

Emission factors were also derived using the box model for the inorganic components detected with Ion Chromatography and PIXE. These are given in Table 3, the values are averaged for both sooting and steady burn. It appeared that the composition of the ultrafine particles were similar in these two burning modes. The compounds responsible for the high inorganic emissions from candle I are phosphates, particularly of ammonium and to a lesser degree potassium. Very low metal emissions were found for candle I. To identify the source of the phosphate particles, samples of wicks and wax were analyzed using PIXE. We found a strong phosphorus signal from the wick of candle I, while phosphorus levels from the wax were below the detection limit. Therefore we conclude that the ultrafine particles emitted from candle I mainly consist of phosphates and that the source of these particles is additives to the wick, likely in the

form of ammonium phosphate added as a flame retardant to the wick. The molar ratio NH_4^+/PO_4^{3-} calculated from the IC data was 1.15 ± 0.15 suggesting that the particles mainly consist of $NH_4H_2PO_4$.

For candle II, the main inorganic compounds detected were potassium, sodium and nitrate. Also several metals were detected using PIXE. The main metal compounds detected were Cu, Sn and Co. These may be from wick hardeners or from additives to the wax, such as color pigments. Candle II was a dark blue candle, perhaps the detected Cu and Co originated from color pigments. Only Zn was detected with PIXE at very low levels in the wick, while the other compounds were below the detection limit (Sn was not analysed in the wick measurements), no compound was detected with PIXE in the wax. It is likely that the metals occur in low concentrations in wax and/or wick and are strongly enriched in the fine particles.

When evaluating an ion balance using the detected compounds in the particle samples it becomes clear that there are missing negative ions not analysed. Another very common flame retardant used in candle wicks is BORAX™. BORAX mainly consists of sodium salts of boron, denoted borates. Neither PIXE, nor the IC techniques used in this study allowed analysis of boron containing compounds. We conclude that the ultrafine particles emitted during steady burn of candle II consist of nitrates of potassium and sodium, metals and non-identified components not analyzed using IC and PIXE.

The observation that the composition of particle emissions from a combustion source can be dominated by water-soluble salts during favourable combustion and that increasing quantities of OC/EC is added during adverse combustion conditions is similar to that found in solid biofuel combustion (Wierzbicka et al. 2005, Pagels et al. 2003)

3.5. On-line measurement of particle volatility

Experiments with the TD placed upstream the SMPS enabled us to make indirect measurements of the composition of the ultrafine particles while still airborne. The decrease in particle (effective) volume as a

function of heater temperature is given in Figure 7. It can be seen that ultrafine particles from candle I are effectively evaporated at around 150 °C and that the remaining particles have a volume less than 5% of the original particle. This is in agreement with particles from candle I being almost pure ammonium phosphate. Di-ammonium-phosphate, $(NH_4)_2HPO_4$ decomposes at 155 °C (Lide, 2008).

A completely different volatility spectra was found for ultrafine particles from candle II. These particles were only marginally affected at temperatures below 350 °C. But a strong decrease in particle volume was found between 350 and 425 °C. Potassium nitrate decomposes at 400 °C (Lide, 2008), which is in excellent agreement with the identified volatility. The remaining volume at 425 °C could be metal compounds or non-analysed components, such as compounds containing boron. The slight decrease below 100 °C may be water bound as crystal water, but could also represent small amounts of organic carbon or a more volatile salt such as ammonium nitrate.

Elemental carbon is non-volatile at temperatures up to at least 550 °C, while organic carbon is mainly volatile below 100-150 °C. These data therefore ensure that the fraction of EC in ultrafine particles from candle I is negligible and that the fraction of OC at least in candle II is low. In the analysis only particles below 150 nm were included, thus excluding any interference with particles in the larger soot mode. Similar measurements were also performed during sooting burn. It was found that the volatilities and thereby the composition of the ultrafine particles was similar to the steady burn experiments, thus even during sooting burn the composition of the ultrafine particles is mainly inorganic and EC/soot is almost entirely emitted as larger particles. These measurements allowed us to verify the composition of the ultrafine particles through measurements on gasborne particles, excluding uncertainties in filter measurements such as evaporation and gas phase adsorption.

Another aim of using the Volatility-SMPS system was to ensure that the two candles brands studied here were representative. A screening study was performed using eight different candle brands. Three of these

emitted ultrafine particles with volatilities similar to candle I and five with volatilities similar to candle II. The size distributions (without TD) from these eight candles were also qualitatively similar to that of candle I and II. Using the SMPS and the V-SMPS we could therefore, without the need to wait for time-consuming chemical analysis, ensure that both in terms of number concentration, size and composition the selected candles were representative of candles sold in Scandinavia.

3.6. Chemically resolved particle size distribution

Samples for size resolved chemical composition analysis were collected using the SDI-Impactor and analysed using PIXE. The results are given in Figure 8. The impactor fractionates the mass concentration into twelve stages according to the aerodynamic equivalent diameter rather than the mobility diameter, which is determined by the SMPS. The only components detected above the detection limit in more than one impactor stage for candle I were phosphorus and potassium (only elements with atomic numbers larger than 12 can be detected with PIXE, so carbon, nitrogen and sodium for example can not be detected). These two components (P and K) have similar size distribution and virtually all emissions occur at sizes below 1 μm, as expected for an aerosol generated through evaporation followed by condensation. For candle II the only detected components in the impactor measurements were potassium, tin and copper, also in this case virtually all detected mass was below 1 μm. The size distribution is similar for potassium and the metals. This suggests that heavy metals emitted from candles occur to a large extent in the same particles as the continuously emitted inorganic ultrafine particles and are perhaps to a lesser degree associated with the larger soot and organics dominated particles emitted during sooting burn and smouldering.

3.7. Mass closure of SMPS, TEOM and filter measurements

The data reduction procedure to calculate mass concentrations and mass size distributions is illustrated in Figures 9 and 10 for an example of an experiment involving candle II during steady burn. First the experimental “effective” volume distribution is determined by weighing the number size distribution by

volume. Then three lognormal size modes are fitted to the effective volume distribution using the least-squares fitting procedure. Two modes need to be used for the ultrafine particles since a smaller mode of freshly produced particles and a larger mode of particles formed by self-coagulation occur. For the soot particles a single mode is sufficient. It can be seen in Figure 9 that a satisfactory fit to the experimental data can be obtained using these three lognormal modes.

To generate the mass size distribution, the effective density of particles in each mode needs to be known. We used a combination of empirical data from the literature and this study. Effective density data from Park et al. (2003) for diesel soot was used for the soot mode. A fractal dimension of 2.4 and an effective density which equals 0.4×10^3 kg m^{-3} at 300 nm was used. Using a fractal dimension smaller than 3.0 leads to a decreasing effective density with increasing particle size.

The effective density was assumed to be the same for the two ultrafine modes with a constant value for all particle diameters. We performed a few Hygroscopic Tandem DMA measurements which showed that the ultrafine particles from candles contain 10-15% water and are therefore likely to be spherical or at least compact liquid droplets at the 30% RH used in the chamber. This would inhibit any agglomerate formation, suggesting that a size-independent effective density may be suitable.

The effective density of the soot mode was held fixed according to the values by Park et al. (2003). The effective density of the ultrafine modes was then varied, until the best fit of the total mass concentration from the SMPS agreed with the mass concentration of the TEOM. The fitted values for the ultrafine particle modes were $1.6 \pm 0.2 \times 10^3$ kg m^{-3} for candle I and $1.5 \pm 0.2 \times 10^3$ kg m^{-3} for candle II. This is lower than the bulk densities of the compounds making up the particles (mono-ammonium phosphate has a density of 1.8×10^3 kg m^{-3} and potassium nitrate has a density of 2.1×10^3 kg m^{-3}), (Lide, 2008). When these values are known, the mass size distribution can be determined as illustrated in Figure 10. The low effective density of soot (below 0.3×10^3 kg m^{-3} near the mass distribution peak at 600 nm) reduces the

magnitude of the soot mode compared to the ultrafine modes when going from the effective volume distribution (Figure 9) to the mass size distribution (Figure 10). Effective volume distributions or mass distributions, where a constant effective density of 1.0×10^3 kg m^{-3} is assumed are often used in the literature to estimate volume or mass concentrations. It should be noted that the volume or mass concentration of soot agglomerates from candles are over-estimated by more than a factor of three using such approaches.

To determine the effective density of the organic particles from smouldering, first the fitted density of the ultrafine particles from the steady burn experiments was used for the ultrafine modes. Then the effective density of the larger OC dominated mode was fitted to be $1.1 \pm 0.2 \times 10^3$ kg m^{-3}, which is slightly higher than the value for pure paraffin and stearic acid (around 0.9×10^3 kg m^{-3}).

In Figure 11 the three different methods to determine the total mass concentration are compared. The methods consisted of: 1) the mass concentration from the TEOM, 2) the size-integrated SMPS mass concentration and 3) filter mass concentration obtained by adding the concentrations of EC, organics and all inorganics detected with PIXE and IC. It can be seen that the total concentration of the three methods is in most cases within 25%, which has to be considered satisfactory. Slightly larger differences were found between filter and TEOM measurements during steady burn of candle II. Presumably due to low concentrations collected onto the filters. Given are also mass concentrations of the three major classes of chemical compounds and ultrafine and fine modes fitted to the SMPS data. It can be seen that the agreement between the concentration of Filter-EC and the fine mode is good in “sooting burn” experiments. Thus the effective density for fractal-like diesel soot particles can be used to accurately describe the mass-mobility relationship of candle soot, even though the candle soot agglomerates are larger than diesel soot.

The agreement between organics and the fine mode is satisfactory during smouldering experiments. The inorganic concentration is slightly higher than the SMPS-ultrafine mode, the reason for this is not clear. The discrepancy was larger during sooting burn. Perhaps this is due to some inorganics being transferred to the soot mode through coagulation. As shown by Pagels et al. (2008) soot particles retain their complex morphology when modest additional material is transferred to the particles as the particles age. This is reflected by the low effective density and complex morphology of the candle soot.

4 Conclusions - implications and recommendation for manufacturers and users

The large differences in composition, particle size and effective density between the different modes in the particle size distribution of candle emissions illustrate that distinctly different particle types are emitted during the different modes of candle burning. This has important implications for potential adverse health effects.

Candles emit ultrafine particles resulting in comparatively high number concentrations in indoor air and these particles mainly consist of inorganic salts. The water-soluble nature of ammonium phosphate and alkali nitrates dominating the composition of the ultrafine particles is an important observation. There are suggestions that the number or surface area concentration of *insoluble* fine particles may be a more relevant dose metric than particle mass (Maynard 2001). The number concentration of ultrafine particles from candles is very high. However, the mass emission factors (which for soluble particles may be the most relevant dose metric) associated with the ultrafine mode is only moderate. Thus potential adverse health effects of particles emitted from steady burning candles may be less than expected from number concentration measurements.

Another implication of the water-soluble nature of these combustion particles is that they grow due to water-uptake in the humid respiratory tract (Rissler et al. 2005), thus decreasing the diffusion coefficient and the deposition probability. For example, hygroscopic NaCl particles of 30 nm have a more than two

times lower deposition probability in the respiratory tract compared to hydrophobic oil particles of the same dry size (Löndahl et al. 2007). However, as shown for candle II in this study, these ultrafine particles may contain metals. Metals have been suggested to be mediators of adverse health effects associated with ultrafine particles. Measurements of both total number concentrations and metal content is strongly recommended to manufacturers. By choosing alternative flame retardants and other additives it may be possible to strongly decrease both the number and mass emission factors during steady burn.

During sooting burn, candles emit relatively high levels of elemental carbon (EC). Candle soot show similarities to diesel soot in terms of morphology. One important difference is that diesel soot often contains a substantial fraction of condensed organic carbon, of which some may be important for adverse health effects, for example Poly Aromatic Hydrocarbons (PAHs). Lau et al. (1997) found comparatively low PAH emissions from candles. However, a more detailed study of PAH emissions also needs to be done during strongly sooting conditions. Another difference between candle soot and diesel soot is that candle soot agglomerates have substantially larger mobility diameters and therefore a lower deposition probability in the respiratory tract. It should be noted that present deposition models assume spherical particles and have not been validated for highly agglomerated soot particles. Hygroscopic material can be transferred to the soot through coagulation in indoor air. Condensed hygroscopic material can transform the particles to more compact forms within the respiratory tract due to uptake of water (Zhang et al. 2008). There is a strong need to establish relevant and meaningful industry standards for EC emission measurements from candles using relevant convective air flows, similar to that what might occur in real indoor settings. For example in the future it may be plausible that candles are labeled with a “sooting index”.

The magnitude of soot exposures from candles is poorly known today. Therefore there is a need for field measurements of EC associated with candle emissions. The magnitude of soot emissions is strongly dependent on the convective air flow patterns in indoor air. Some studies suggest that candles can make a

relatively strong contribution to the personal exposure to EC (Sorensen et al. 2005, Ogden et al. 2000). It should be pointed out that most soot emissions from candles can be avoided by using high-quality candles, trimming long wicks and by avoiding burning candles when air flows are so high that the candle flame flickers or even visible soot plumes appear.

Acknowledgements: The work was supported by the Swedish research council FORMAS and SBUF, The construction industry's organisation for research and development

References

Afshari,A., Matson,U., Ekberg,L.E., 2005. Characterization of indoor sources of fine and ultrafine particles: a study conducted in a full-scale chamber, *Indoor Air* 15, pp. 141-150.

Burtscher,H., Baltensperger,U., Bukowiecki,N., Cohn,P., Huglin,C., Mohr,M., Matter,U., Nyeki,S., Schmatloch,V., Streit,N., Weingartner,E., 2001. Separation of volatile and non-volatile aerosol fractions by thermodesorption: instrumental development and applications, *Journal of Aerosol Science* 32, pp. 427-442.

Chow,J.C., Watson,J.G., Pritchett,L.C., Pierson,W.R., Frazier,C.A., Purcell,R.G., 1993. The Dri Thermal Optical Reflectance Carbon Analysis System - Description, Evaluation and Applications in United-States Air-Quality Studies, *Atmospheric Environment Part A-General Topics* 27, pp. 1185-1201.

Edwards,H.G.M., Farwell,D.W., Brooke,C.J., 2005. Raman spectroscopic study of a post-medieval wall painting in need of conservation, *Analytical and Bioanalytical Chemistry* 383, pp. 312-321.

Fan,C.W., Zhang,J.J., 2001. Characterization of emissions from portable household combustion devices: particle size distributions, emission rates and factors, and potential exposures, *Atmospheric Environment* 35, pp. 1281-1290.

Fine,P.M., Cass,G.R., Simoneit,B.R.T., 1999. Characterization of fine particle emissions from burning church candles, *Environmental Science & Technology* 33, pp. 2352-2362.

Heidam,N.Z., 1981. Review - Aerosol Fractionation by Sequential Filtration with Nuclepore Filters, *Atmospheric Environment* 15, pp. 891-904.

Hussein,T., Glytsos,T., Ondracek,J., Dohanyosova,P., Zdimal,V., Hameri,K., Lazaridis,M., Smolik,J., Kulmala,M., 2006. Particle size characterization and emission rates during indoor activities in a house, *Atmospheric Environment* 40, pp. 4285-4307.

Huynh,C.K., Savolainen,H., Vuduc,T., Guillemin,M., Iselin,F., 1991. Impact of Thermal Proofing of A Church on Its Indoor Air-Quality - the Combustion of Candles and Incense As A Source of Pollution, *Science of the Total Environment* 102, pp. 241-251.

Klepeis,N.E., Nelson,W.C., Ott,W.R., Robinson,J.P., Tsang,A.M., Switzer,P., Behar,J.V., Hern,S.C., Engelmann,W.H., 2001. The National Human Activity Pattern Survey (NHAPS): a resource for assessing exposure to environmental pollutants, *Journal of Exposure Analysis and Environmental Epidemiology* 11, pp. 231-252.

Knight,L., Levin,A., Mendenhall C., 2001. Candles and Incense as potential sources of indoor air pollution: market analysis and literature review, *United States Environmental Protection Agency*, National Risk Management Research Laboratory Cincinnati, Ohio 45268.

Koutrakis,P., Brauer,M., Briggs,S.L.K., Leaderer,B.P., 1991. Indoor Exposures to Fine Aerosols and Acid Gases, *Environmental Health Perspectives* 95, pp. 23-28.

Larosa,L.B., Buckley,T.J., Wallace,L.A., 2002. Real-time indoor and outdoor measurements of black carbon in an occupied house: An examination of sources, *Journal of the Air & Waste Management Association* 52, pp. 41-49.

Lau,C., Fiedler,H., Hutzinger,O., Schwind,K.H., Hosseinpour,J., 1997. Levels of selected organic compounds in materials for candle production and human exposure to candle emissions, *Chemosphere* 34, pp. 1623-1630.

Li,W., Hopke,P.K., 1993. Initial Size Distributions and Hygroscopicity of Indoor Combustion Aerosol-Particles, *Aerosol Science and Technology* 19, pp. 305-316.

Lide,D.,R., ed., 2008. CRC Handbook of Chemistry and Physics, 88th Edition (Internet Version 2008), CRC Press/Taylor and Francis, Boca Raton, FL, USA.

Lin,T.S., Shen,F.M., Chen,J.L., Yang,M.H., 2003. Trace metals in candle smoke, *Bulletin of Environmental Contamination and Toxicology* 70, pp. 182-187.

Londahl,J., Massling,A., Pagels,J., Swietlicki,E., Vaclavik,E., Loft,S., 2007. Size-resolved respiratory-tract deposition of fine and ultrafine hydrophobic and hygroscopic aerosol particles during rest and exercise, *Inhalation Toxicology* 19, pp. 109-116.

Long,C.M., Suh,H.H., Koutrakis,P., 2000. Characterization of indoor particle sources using continuous mass and size monitors, *Journal of the Air & Waste Management Association* 50, pp. 1236-1250.

Martinsson,B.G., Karlsson,M.N.A., Frank,G., 2001. Methodology to estimate the transfer function of individual differential mobility analyzers, *Aerosol Science and Technology* 35, pp. 815-823.

Matson,U., 2005. Indoor and outdoor concentrations of ultrafine particles in some Scandinavian rural and urban areas, *Science of the Total Environment* 343, pp. 169-176.

Maynard,A.D., Maynard,R.L., 2002. A derived association between ambient aerosol surface area and excess mortality using historic time series data, *Atmospheric Environment* 36, pp. 5561-5567.

Nriagu,J.O., Kim,M.J., 2000. Emissions of lead and zinc from candles with metal-core wicks, *Science of the Total Environment* 250, pp. 37-41.

Ogulei,D., Hopke,P.K., Wallace,L.A., 2006. Analysis of indoor particle size distributions in an occupied townhouse using positive matrix factorization, *Indoor Air* 16, pp. 204-215.

Pagels,J., Strand,M., Rissler,J., Szpila,A., Gudmundsson,A., Bohgard,M., Lillieblad,L., Sanati,M., Swietlicki,E., 2003. Characteristics of aerosol particles formed during grate combustion of moist forest residue. *Journal of Aerosol Science* 34, pp. 1043-1059.

Pagels J., Khalizov A., McMurry PH. and Zhang RY., (2008) Processing of Soot by Controlled Sulphuric Acid and Water Condensation – Mass and Mobility Relationship. Accepted for publication in Aerosol Science and Technology.

Park,K., Cao,F., Kittelson,D.B., McMurry,P.H., 2003. Relationship between particle mass and mobility for diesel exhaust particles, *Environmental Science & Technology* 37, pp. 577-583.

Park,K., Kittelson,D.B., McMurry,P.H., 2004. Structural properties of diesel exhaust particles measured by transmission electron microscopy (TEM): Relationships to particle mass and mobility, *Aerosol Science and Technology* 38, pp. 881-889.

Perez,F.R., Edwards,H.G.M., Rivas,A., Drummond,L., 1999. Fourier transform Raman spectroscopic characterization of pigments in the mediaeval frescoes at Convento de la Peregrina, Sahagun, Leon, Spain. Part 1 - Preliminary study, *Journal of Raman Spectroscopy* 30, p. 301-+.

Rissler,J., Pagels,J., Swietlicki,E., Wierzbicka,A., Strand,M., Lillieblad,L., Sanati,M., Bohgard,M., 2005. Hygroscopic behavior of aerosol particles emitted from biomass fired grate boilers, *Aerosol Science and Technology* 39, pp. 919-930.

Sakurai,H., Park,K., McMurry,P.H., Zarling,D.D., Kittelson,D.B., Ziemann,P.J., 2003. Size-dependent mixing characteristics of volatile and nonvolatile components in diesel exhaust aerosols, *Environmental Science & Technology* 37, pp. 5487-5495.

Sorensen,M., Loft,S., Andersen,H.V., Nielsen,O.R., Skovgaard,L.T., Knudsen,L.E., Ivan,V.N.B., Hertel,O., 2005. Personal exposure to PM2.5, black smoke and NO2 in Copenhagen: relationship to bedroom and outdoor concentrations covering seasonal variation, *Journal of Exposure Analysis and Environmental Epidemiology* 15, pp. 413-422.

Zai. S., Huang,Z., Wang,J.S., 2006. Studies on the size distribution, number and mass emission factors of candle particles characterized by modes of burning, *Journal of Aerosol Science* 37, pp. 1484-1496.

van Alphen,M., 1999. Emission testing and inhalational exposure-based risk assessment for candles having Pb metal wick cores, *Science of the Total Environment* 244, pp. 53-65.

Wasson,S.J., Guo,Z.S., McBrian,J.A., Beach,L.O., 2002. Lead in candle emissions, *Science of the Total Environment* 296, pp. 159-174.

Wierzbicka,A., Lillieblad,L., Pagels,J., Strand,M., Gudmundsson,A., Gharibi,A., Swietlicki,E., Sanati,M., Bohgard,M., 2005. Particle emissions from district heating units operating on three commonly used biofuels, *Atmospheric Environment* 39, pp. 139-150.

Wierzbicka A., Gudmundsson A., Pagels J., Dahl A., Löndahl J., Swietlicki E. and Bohgard M. 2008. Characteristics of Airborne Particles in Various Swedish Indoor Environments. Paper I in *What Are the Characteristics of Airborne Particles that We Are Exposed to? Focus on Indoor Environments and Emissions from Biomass Fired District Heating*, PhD Thesis, Lund University 2008

Zhang RY., Khalizov AF., Pagels J., Zhang DD., Xue H., J. Chen and McMurry PH. (2008) Variability in morphology, hygroscopicity and optical properties of soot aerosols during internal mixing in the atmosphere. Proceedings of the National Academy of Sciences of the United States of America. 30: 10291-10296

1

FIGURE CAPTIONS

Figure 1. Schematic figure of experimental set-up

Figure 2. Average number particle size distributions in the 21.6 m^3 chamber during steady and sooting burn of 4 candles. Air exchange rate was 0.5 h^{-1}.

Figure 3. lnfluence of smouldering emissions upon candle extinction on the particle number size distribution. Four candles of type II were burning for 10 min before extinguishing. Average of three repeated experiments. The air exchange rate was 0.5 h^{-1}.

Figure 4. TEM images of particles in the soot mode at different magnification. Candle II, “sooting” combustion.

Figure 5. Chemical composition of candle smoke for the two candle types at different burning conditions, given as average mass concentration in the chamber over a period of 60 minutes after the candle is either lighted (sooting and steady burn) or extinguished (smoulder). Note that the EC - concentration during sooting burn for candle II extends out of scale and the value is 1424 $\mu g/m^3$.

Figure 6. Experimental and modeled mass concentrations in the chamber during a steady burn experiment for candle II, TEOM data (PM2.5). The modeled concentration and fitted emission factor was obtained using the least squares optimization procedure.Wall losses were modeled in two different ways, 1. using the average GMD of the whole experiment to estimate losses or 2. using the GMD of each SMPS scan (time dependent losses).

Figure. 7. The remaining volume fraction as a function of temperature. A thermodesorber was used upstream the SMPS, “Steady Burn” experiments.

Figure 8. Aerodynamic particle size distribution of major elements detected in steady burn experiments with four candles burning in the chamber. Left: Candle I, Right: Candle II. Samples collected with the SDI impactor and analyzed using PIXE.

Figure 9. "Effective" volume distribution, with three fitted lognormal modes. Example for Candle II, steady burn.

Figure 10. Assessed mass distribution of SMPS measurements, with three fitted lognormal modes. Example for Candle II during steady burn. An effective density of 1.5×10^3 kg m^{-3} was used for the two ultrafine modes and a size dependent effective density used for the "soot" mode (Park et al. 2003).

Figure 11. Comparison of mass concentrations obtained from TEOM, filter and SMPS. For SMPS measurements the empirically determined effective densities were used. Measurements during sooting burn of candle II were multiplied by 0.5 to fit the scale.

TABLE

Table 1. Summary of deduced emission factors of candle smoke particles (for a single candle). Comparisons to literature data. Uncertainties given as standard deviations of repeated measurements. PM2.5 mass measured independently using the TEOM.

Candle Type – Burn Mode	Reference	PM2.5 mass (mg h^{-1})	Elemental Carbon (mg h^{-1})	Organic Matter (mg h^{-1})	Inorganic Compounds (mg h^{-1})
Candle I – Steady Burn	This study	2.4 ± 0.1	0.14 ± 0.11	0.04 ± 0.06	2.9 ± 0.5
Candle II – Steady Burn	This study	0.87 ± 0.14	0.31 ± 0.36	0.05 ± 0.07	0.92 ± 0.34
Paraffin candle - Steady Burn	Zai et al. 2006	0.33 ± 0.03	-	-	-
Candle I – Sooting	This study	8.9 ± 0.4	4.5 ± 0.2	0.24 ± 0.33	3.3 ± 0.6
Candle II – Sooting	This study	25.3 ± 0.02	19.0 ± 0.6	1.3 ± 0.3	1.1 ± 0.6
Paraffin candle - Sooting	Fine et al. 1999	26.6	24.1	1.4	-
Paraffin candle - Sooting	Zai et al. 2006	7.6 ± 2.2	-	-	-

Table 2. Summary of deduced emission factors of candle smoke particles. Smouldering emissions given as mg particles released upon a single extinction of a single candle, comparisons to literature data. Uncertainties given as standard deviations of repeated measurements.

Candle Type – Burn Mode	Reference	PM2.5 mass (mg)	Elemental Carbon (mg)	Organic Matter (mg)	Inorganic Compounds (mg)
Candle II – Smoulder	This study	0.72 ± 0.04	0.03 ± 0.01	0.80 ± 0.03	0.11± 0.06
Paraffin candle - Smoulder	Fine et al. 1999	0.65 ± 0.14	0.05 ± 0.05	0.82 ± 0.19	-
Beeswax candle – Smoulder	Fine et al. 1999	1.7 ± 0.35	<0.04	1.9 ± 0.36	-
Paraffin candle - Smoulder	Zai et al. 2006	0.24 ± 0.07	-	-	-

Table 3. Detailed inorganic composition for candle I and II from PIXE (n=2) and IC (n=3) analysis, given as emission factors ($\mu g\ h^{-1}$) for each component. Average of steady and sooting burn experiments for each candle.

	Candle I	**Candle II**
PO_4^{3-}	2300	1
NO_3^-	20	310
SO_4^{2-}	9	5
Cl^-	28	47
F^-	20	23
NH_4^+	490	17
Na^+	45	210
K^+	140	270
Cu	0	80
Sn	1	44
Co	0	19
Zn	0	2
Pb	0	3
Sum	**3060**	**1030**

FIGURES

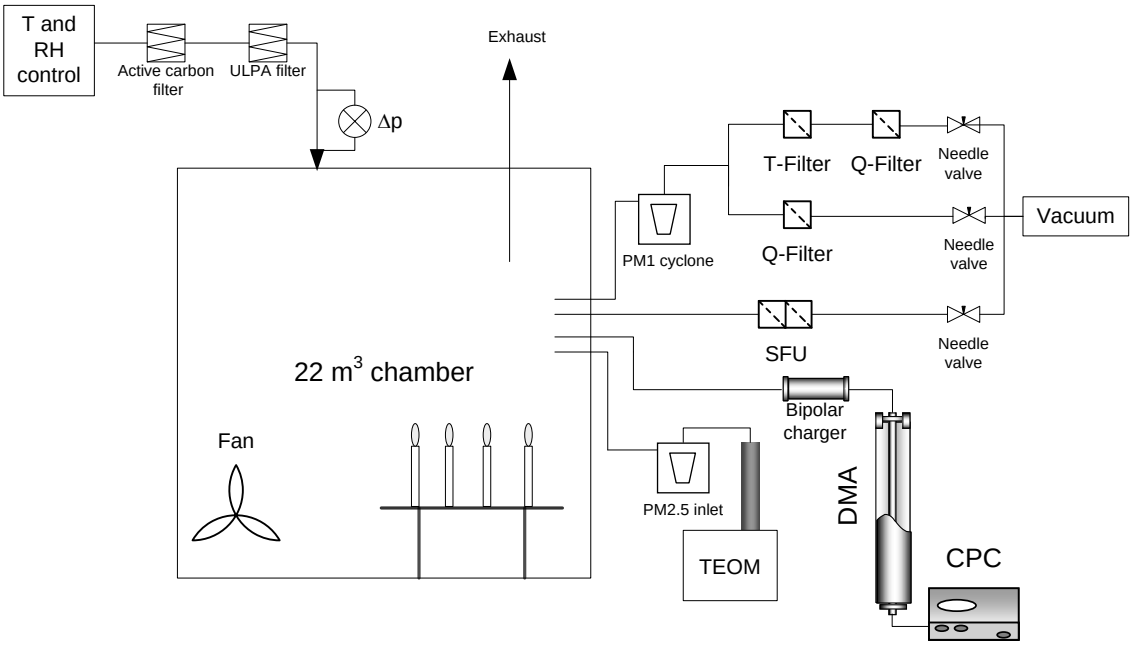

Figure 1.

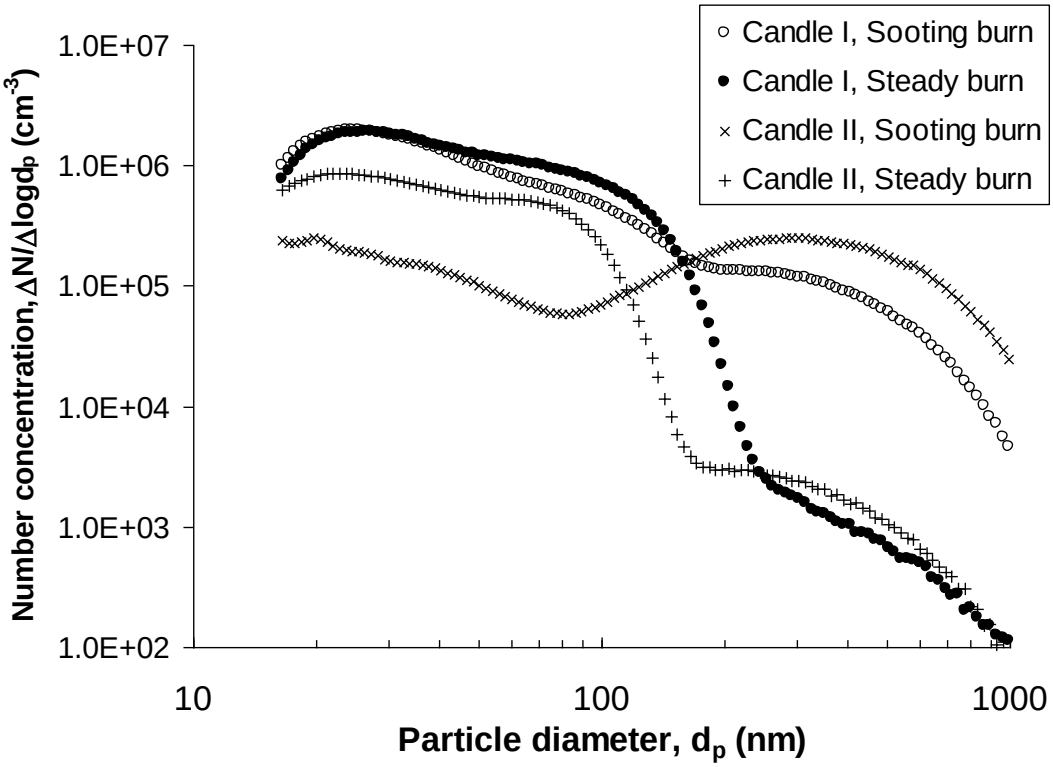

Figure 2.

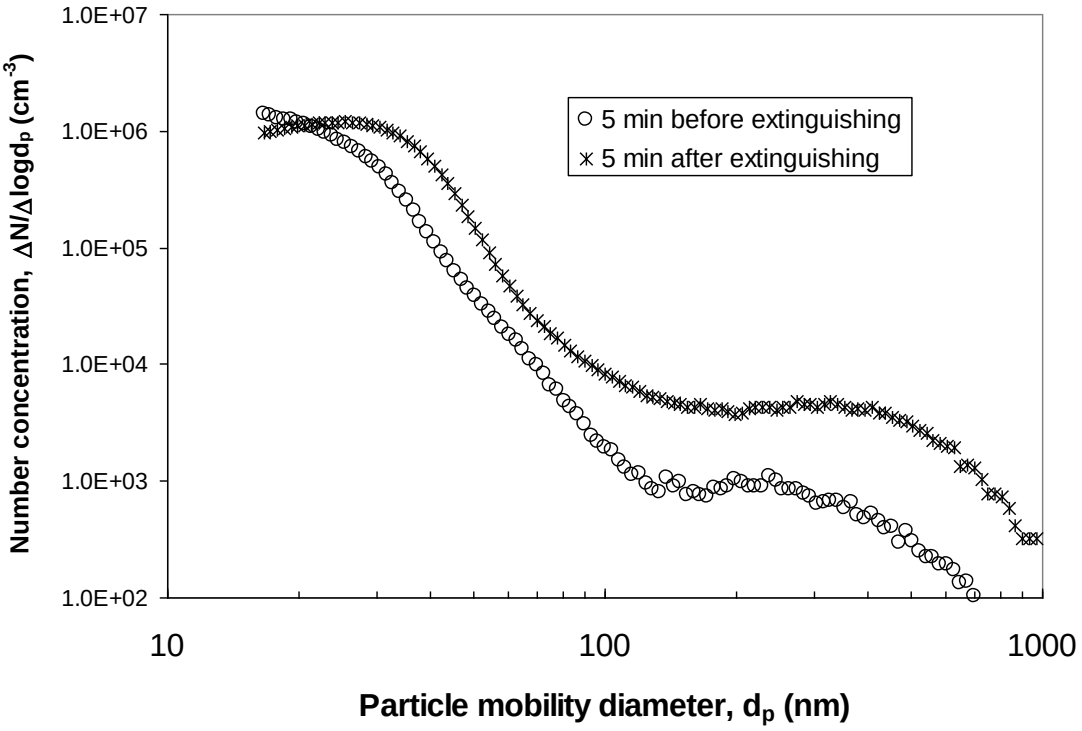

Figure 3.

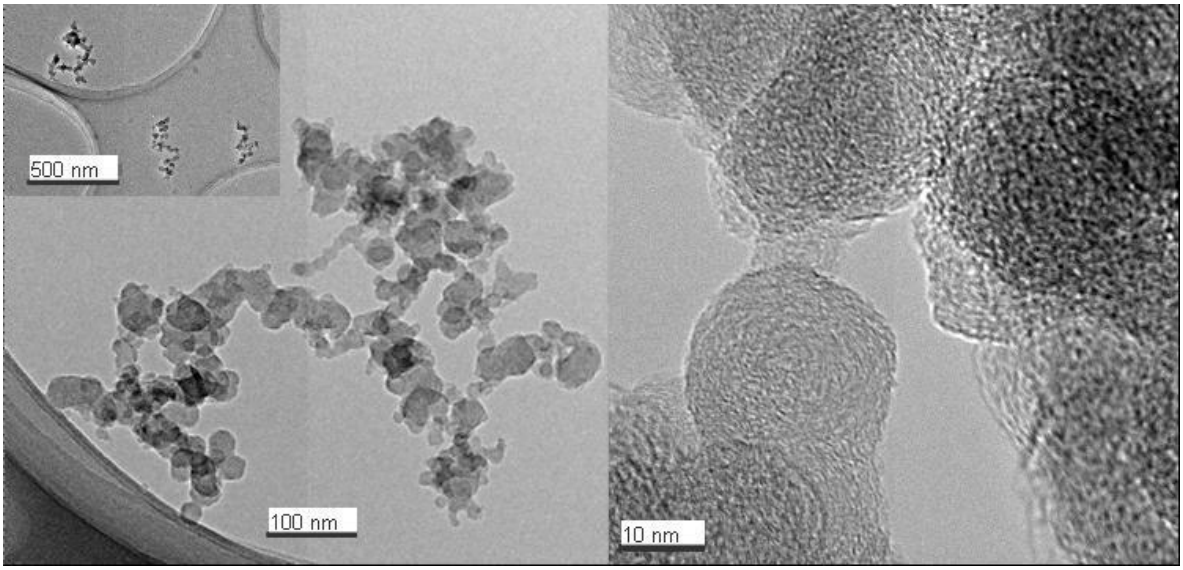

Figure 4.

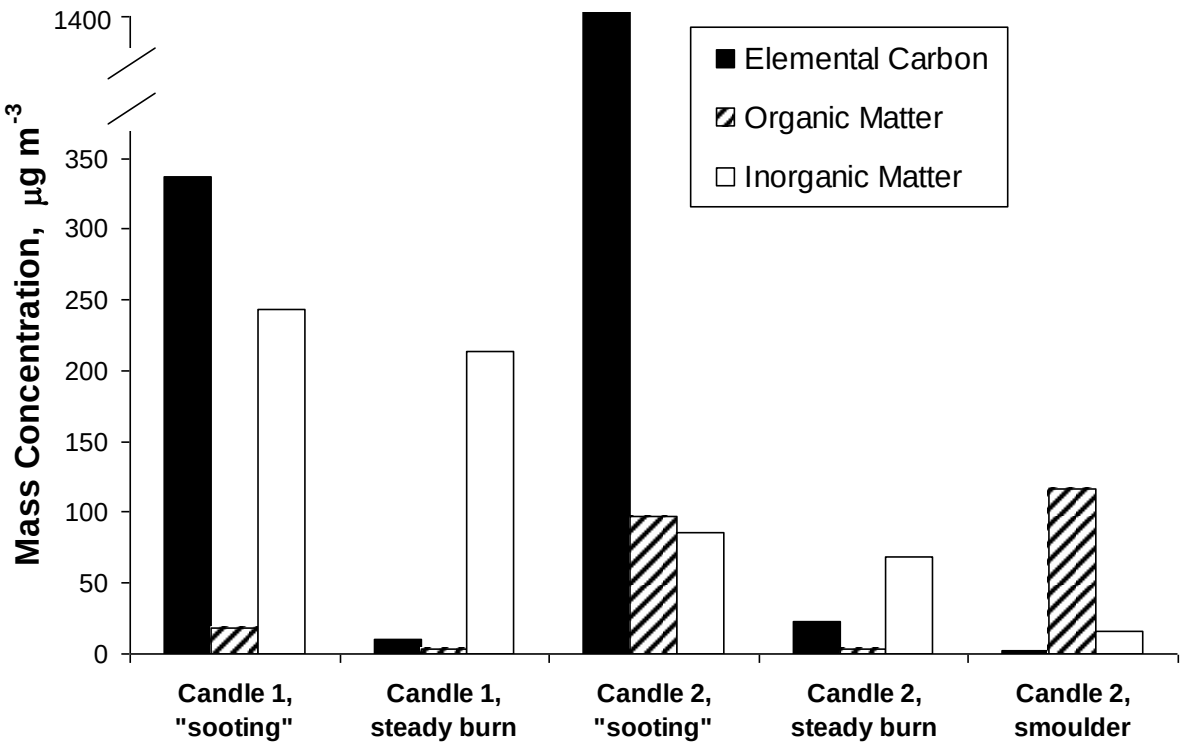

Figure 5.

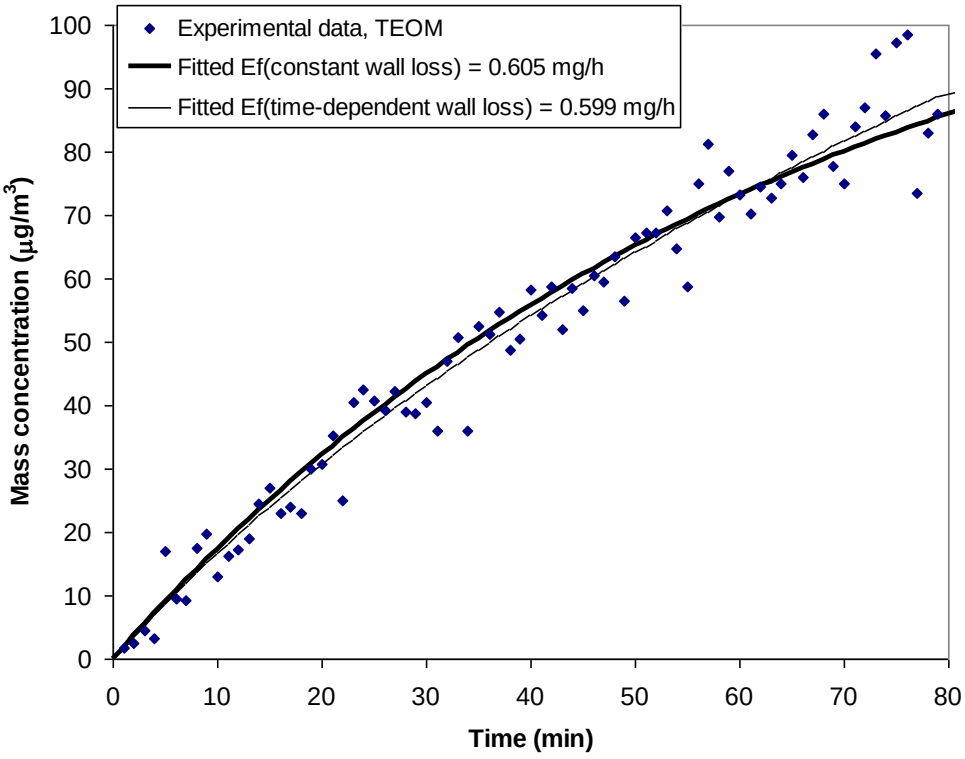

Figure 6

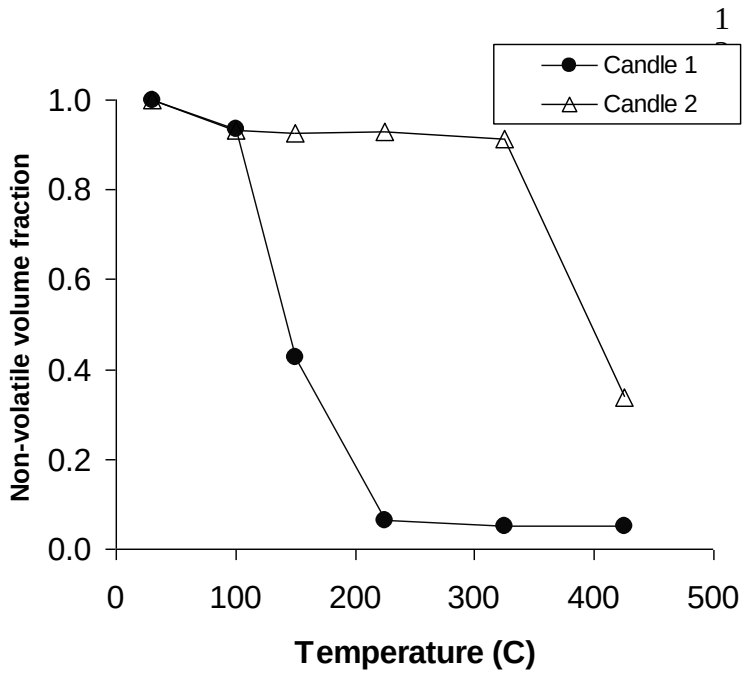

Figure. 7.

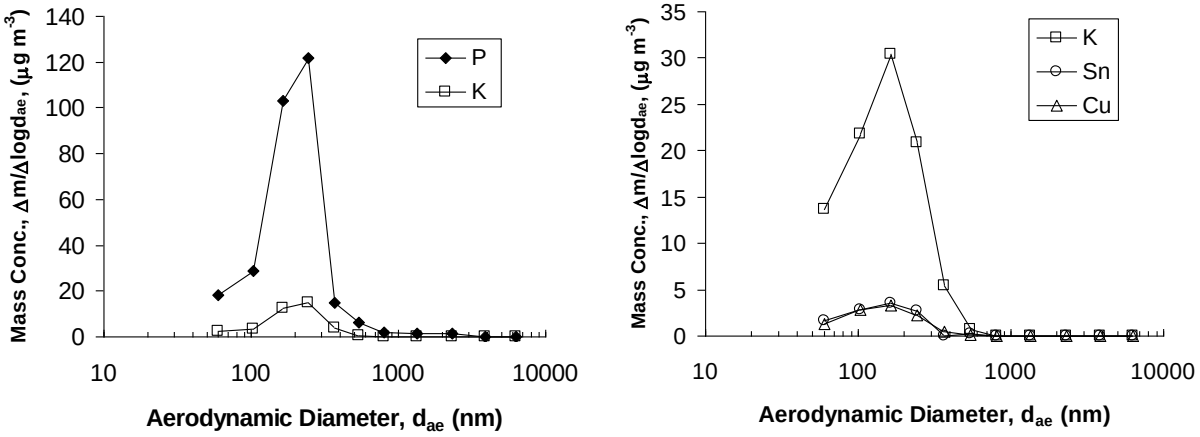

Figure 8.

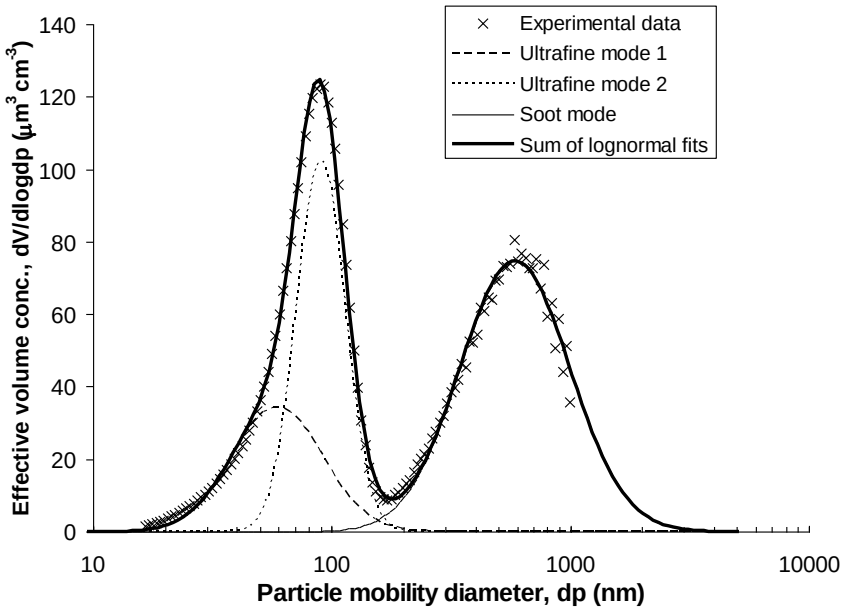

Figure 9.

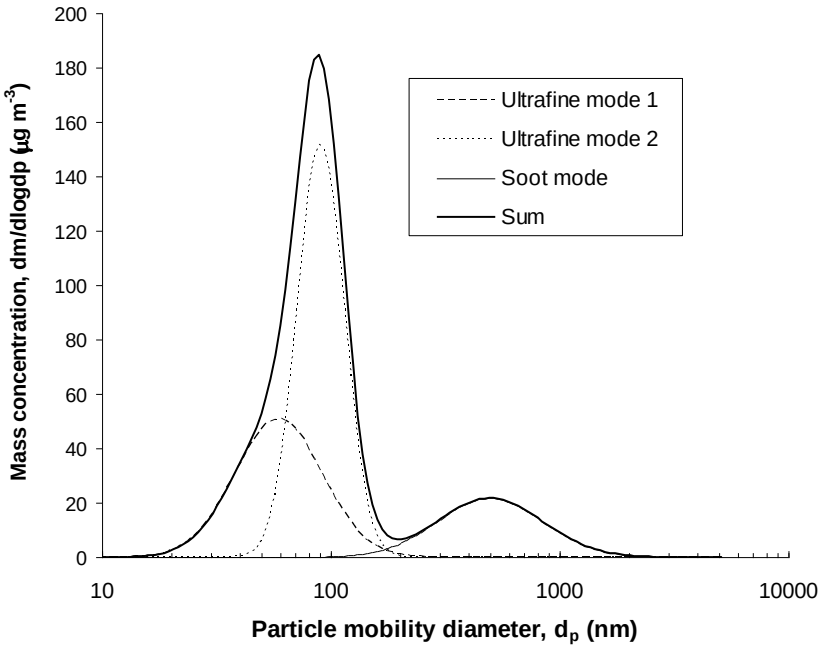

Figure 10.

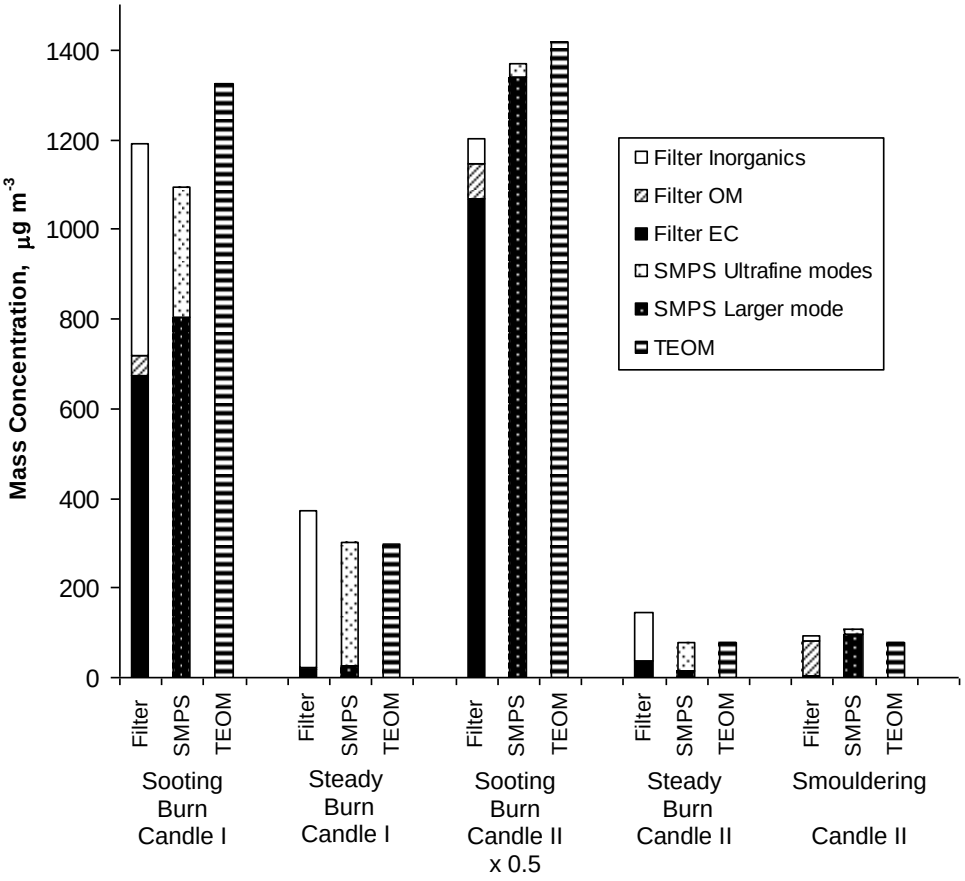
Mass Concentration, µg m-3
1400
1200
1000
800
600
400
200
0
Filter Inorganics
Filter OM
Filter EC
SMPS Ultrafine modes
SMPS Larger mode
TEOM
Filter
SMPS
TEOM
Sooting Burn Candle I
Steady Burn Candle I
Sooting Burn Candle II x 0.5
Steady Burn Candle II
Smouldering Candle II

Figure 11.